

Solving Non-local Fokker-Planck Equations by Deep Learning

Senbao Jiang^{*1} and Xiaofan Li^{†1}

¹Department of Applied Mathematics, Illinois Institute of Technology

June 8, 2022

Abstract

Physics-informed neural networks (PiNNs) recently emerged as a powerful solver for a large class of partial differential equations under various initial and boundary conditions. In this paper, we propose *trapz-PiNNs*, physics-informed neural networks incorporated with a modified trapezoidal rule recently developed for accurately evaluating fractional laplacian and solve the space-fractional Fokker-Planck equations in 2D and 3D. We describe the modified trapezoidal rule in detail and verify the second-order accuracy. We demonstrate trapz-PiNNs have high expressive power through predicting solution with low \mathcal{L}^2 relative error on a variety of numerical examples. We also use local metrics such as pointwise absolute and relative errors to analyze where could be further improved. We present an effective method for improving performance of trapz-PiNN on local metrics, provided that physical observations of high-fidelity simulation of the true solution are available. Besides the usual advantages of the deep learning solvers such as adaptivity and mesh-independence, the trapz-PiNN is able to solve PDEs with fractional laplacian with arbitrary $\alpha \in (0, 2)$ and specializes on rectangular domain. It also has potential to be generalized into higher dimensions.

1 Introduction

The Fokker-Planck equations (FPEs) describe the time evolution of probability density functions of underlying stochastic dynamics [3]. If the driving noise is Gaussian (brownian motions), the FPE is a parabolic partial differential equation involving laplacian. The FPEs are widely used in studying stochastic models in physical, chemical and biological systems. There are many cases that the driving noises are non-Gaussian [2, 19, 18], such as isotropic α -stable Lévy motions, then the corresponding FPEs are non-local parabolic PDE involving fractional laplacian. For a introduction to FPEs, see [3].

We are interested in the following non-local Fokker-Planck Equation defined on $\Omega_T := \Omega \times (0, T)$

^{*}Corresponding Author: sjiang23@hawk.iit.edu

[†]lix@iit.edu

where $\Omega \in \mathbb{R}^n$, $n \geq 1$ is a rectangular domain

$$\partial_t u(x, t) = -\nabla \cdot (f u) + \frac{1}{2} \text{Tr} \{ \nabla^2 : (\sigma(x)\sigma(x)^T u(x, t)) \} - (-\Delta)^{\frac{\alpha}{2}} u(x, t), \quad (x, t) \in \Omega_T, \quad (1)$$

$$u(x, t) = 0, \quad x \notin \Omega, \quad t > 0, \quad (2)$$

$$u(x, 0) = u_0(x). \quad (3)$$

Here, $\alpha \in (0, 2)$, $f(x)$ is a C^2 vector field in \mathbb{R}^n and $\sigma(x)$ is a C^2 $n \times n$ matrix-valued map, the fractional laplacian is defined by

$$(-\Delta)^{\frac{\alpha}{2}} \varphi(x) := c_{n,\alpha} \text{P.V.} \int_{\mathbb{R}^n \setminus \{0\}} \frac{\varphi(x) - \varphi(y)}{|x - y|^{n+\alpha}} dy, \quad (4)$$

$$\text{where } c_{n,\alpha} := \frac{2^\alpha \Gamma(\frac{\alpha+n}{2})}{\pi^{\frac{n}{2}} |\Gamma(-\frac{\alpha}{2})|}. \quad (5)$$

We sometimes denote Eq. (1) by $\partial_t u = \mathcal{L}u$ for convenience. After rescaling, we can always assume $\Omega = (-1, 1)^n$, a hypercube with side length two. For more information about fractional laplacian, we refer to [14].

Finite difference type numerical method for the non-local partial differential equations involving fractional laplacian usually relies on the discretization of fractional laplacian [26, 21, 22, 4, 5, 8]. Recently, a new accurate numerical scheme has been developed for computing fractional laplacian in 2D [11]. It is a modified trapezoidal rule with correction terms around singularity in order to achieve high-order accuracy of the quadrature. The correction weights are pre-computed. Once being stored, the modified trapezoidal rule can be easily set up. Blended with finite difference method, it has been applied to solving one and two dimensional non-local FPEs in [5, 8] respectively. It is not hard to generalize this rule to arbitrary n dimensions. For full presentation of the modified trapezoidal rule in 2D and its convergence analysis, please refer to [11].

Apart from classical methods, the surge of artificial intelligence influenced numerical PDEs community. The Physics-informed Neural Networks (PiNNs) emerged as powerful deep learning solvers for partial differential equations (PDEs) [20, 9, 17], fractional PDEs [15, 16], or stochastic PDEs [25] with various initial and/or boundary conditions. PiNN was formally introduced by Rassi et al [17], in which the authors provided data-driven solution (forward problem) and data-driven discovery (inverse problem) of some integer-order PDEs for continuous time models and discrete time models. PiNN has been further extended to solve nonlocal or fractional type PDEs by incorporating classical numerical methods to evaluate non-local or fractional operators, where the automatic differentiation is not applicable. In [15], Pang et al proposed a unified nonlocal operator encompassing both fractional laplacian and classical laplacian, which is computed in spherical coordinates and Gauss-Legendre quadrature rule. Combining this unified operator with PiNN, they are able to solve non-local Poisson model and non-local turbulence. A parallel work by Pang et al [16] combines PiNN with one-dimensional and multi-dimensional Grunwald-Letnikov numerical schemes and Gauss-Legendre quadrature rule to discretize the fractional laplacian and solves forward and inverse problem of fractional advection-diffusion equations in one, two and three dimensions in circular or spherical domains. Xu et al [23] verifies the PiNN accurately solves the integer-order stationary FPEs in one, two and three dimensions.

In this work we propose the modified-trapezoidal-rule-incorporated Physics-informed Neural Networks and focus on forward problem for the non-local FPEs. We call *trapz-PiNNs* for short, it is sufficient to only use the simplest version of the modified trapezoidal rule: a trapezoidal rule plus

one correction term on singularity and provides second-order accuracy for evaluating the fractional laplacian. The expressive power of trapz-PiNN is demonstrated by accurately predicting the solution of nonlocal FPEs at time T_{pred} after training strictly before the time T for some $T \leq T_{\text{pred}}$. We verify the accuracy of the deep learning (DL) solution by comparing it with reference solution obtained from finite difference method (FDM) under \mathcal{L}^2 relative error. Apart from achieving good global metric \mathcal{L}^2 relative error, we investigate the DL solution profile from local metric such as pointwise absolute and relative errors. It turns out that even achieving good \mathcal{L}^2 relative error, trapz-PiNN predicts more accurately in the regions with large or moderate magnitude than regions with small magnitude. If physical observation of solution data or high-fidelity simulated data is available [15], we propose an effective loss function integrating the extra data into trapz-PiNN framework to further enhance the performance on the local metrics, provided physical observation of solution data or high-fidelity simulated data is available.

It worths mentioning that trapz-PiNN is not limited to being the solver of the non-local FPEs. It can be adapted to other non-local PDEs involving fractional laplacian such as fractional reaction-diffusion equations, Cahn-Hilliard equations etc. Besides the usual advantages of PiNNs such as independence of mesh grids and easy adaptivity, the proposed trapz-PiNN has the following characteristics:

1. trapz-PiNN solves the non-local PDEs on rectangular spacial domains while the previous relevent works emphasize on circular or spherical ones.
2. The numerical scheme for fractional laplacian is valid for arbitrary $\alpha \in (0, 2)$, and so is trapz-PiNN.
3. Although we only provide numerical examples in two or three dimensions in this work, trapz-PiNN can be generalized to higher dimensional settings.

We describe some notations that appear throughout the paper. n denotes spatial dimensions, usually 2, 3 but could be higher. $\Delta t > 0$ represents the time step size and $h > 0$ means space resolution. $|x|$ is the l^2 norm of $x \in \mathbb{R}^n$. $\Omega = (-1, 1)^n$ is a hypercube with side length two and $\Omega_T = \Omega \times (0, T)$ for some $T > 0$. To facilitate reading, Table 1 records all common acronyms used in this paper.

Full word	acronyms
Partial Differential Equations	PDEs
Fokker-Planck Equations	FPEs
Ornstein-Uhlenbeck	O-U
Finite Difference Method	FDM
Neural Network	NN
Physics-informed Neural Networks	PiNNs
Mean Squared Error	MSE
Deep Learning	DL
Stochastic Gradient Descent	SGD

Table 1: Common Acronyms

We organize this paper as follows. In Section 2 we discuss the modified trapezoidal rule and demonstrate the second-order accuracy for approximating the fractional laplacian. We elaborate

the construction of the trapz-PiNNs in Section 3. Numerical results are given in detail in Section 4, in particular, we solve fractional heat equations in 2D and 3D and FPE with Ornstein–Uhlenbeck potential in 2D. We also proposed a modified loss function and compare the DL solution profiles computed by trapz-PiNNs equipped with the original and modified loss functions. Section 5 summarizes the work and present future directions.

2 Numerical Scheme for the Fractional Laplacian

2.1 The modified trapezoidal rule

Accurately computing the fractional laplacian is essential in constructing the loss function in trapz-PiNNs. In this section, we introduce a simplest version of the modified trapezoidal rule introduced in [11]. Let $\phi \in C_c^N(\mathbb{R}^n)$ with $N > \max\{4 - \alpha, n\}$. The modified trapezoidal rule is designed to numerically compute a class of weakly singular integrals, in particular

$$I_\alpha^{(j)} = \int_{\mathbb{R}^n \setminus \{0\}} \phi(x) \frac{x_j^2}{|x|^{n+\alpha}} dx, \quad j = 1, \dots, n. \quad (6)$$

It turns out that discretization of fractional laplacian boils down to evaluating weakly singular integrals (6). See [8, section 3.3]. Let f be a Schwartz function or function with compact support on \mathbb{R}^n , we define punctured-hole trapezoidal rule to be

$$T_h[f] := h^n \sum_{k \in \mathbb{Z}^n, k \neq 0} f(kh). \quad (7)$$

Writing

$$s_j(x) = \frac{x_j^2}{|x|^{n+\alpha}}, \quad (8)$$

the modified trapezoidal rule for $I_\alpha^{(j)}$ is given by

$$Q_h^{(j)}[\phi s_j] = T_h[\phi s_j] + h^{2-\alpha} \omega_0^{(j)} \phi(0). \quad (9)$$

Here, $\omega_0^{(j)}$ is a correction weight that can be computed by the following limit

$$\omega_0^{(j)} = \lim_{h \rightarrow 0} \frac{1}{h^{2-\alpha}} \left(\int_{\mathbb{R}^n \setminus \{0\}} g(x) s_j(x) dx - T_h[g \cdot s_j] \right), \quad (10)$$

where g is a radially symmetric Schwartz function. After a symmetry argument, one can see that

$$\omega_0^{(1)} = \dots = \omega_0^{(n)} =: \omega_0. \quad (11)$$

It is a proven fact that this simple modified trapezoidal rule has order of convergence $4 - \alpha$ for weakly singular integral (6). For more information about the full version of this numerical rule and related convergence analysis, please refer to [11].

2.2 Numerical Fractional Laplacian

The modified trapezoidal rule (9) can be applied to fractional laplacian (4) with second-order accuracy. Let $\varphi(x) \in C_c^N(\mathbb{R}^n)$ with $\text{supp}(\varphi) \subset \Omega$ and let $\Omega_h := (x_k)_k$ be any uniform mesh grid for Ω with mesh size h , then the fractional laplacian evaluated at x_k is approximated by

$$\begin{aligned} (-\Delta)^{\frac{\alpha}{2}}\varphi(x_k) &\approx h^n c_{n,\alpha} \sum''_{x_l \in \Omega_h \setminus \{x_k\}} \frac{\varphi(x_k) - \varphi(x_l)}{|x_k - x_l|^{n+\alpha}} - \frac{1}{2} c_{n,\alpha} \omega_0 h^{2-\alpha} \sum_{j=1}^n \partial_{jj}^2 \varphi(x_k) \\ &+ c_{n,\alpha} \varphi(x_k) I_\alpha(x_k), \end{aligned} \quad (12)$$

where \sum''_{x_l} indicates the summand is divided by 2^m if grid point x_l lies on m edges and

$$I_\alpha(x) := \int_{\Omega^c} \frac{dy}{|y - x|^{n+\alpha}} \quad (13)$$

can be evaluated analytically. In particular, the analytical formula for Eq. (13) in 2D is available in [8]. We denote the discretized fractional laplacian (the RHS of Eq. (12)) by $(-\Delta)_h^{\alpha/2}$.

We now verify the second-order accuracy of Eq. (12) in 2D, while the verification in other dimensions are similar. Let

$$\phi(x) := (1 + x_1 + 2x_1^2)(1 + x_2^2)(1 - x_1^2)_+^5(1 - x_2^2)_+^5 \in C_c^4(\mathbb{R}^2) \quad (14)$$

so that $\text{supp}(\phi) = [-1, 1]^2$. In 2D the correction weight ω_0 is given by

$$\omega_0 = \begin{cases} 0.960844610589965, & \alpha = 0.5 \\ 1.950132460000978, & \alpha = 1 \\ 5.038779739396576, & \alpha = 1.5 \end{cases} \quad (15)$$

We compute $(-\Delta)_h^{\alpha/2} \phi(x)$ at $x = (0.25, -0.125), (0.875, 0.25), (0.375, -0.625)$ for each $h = \frac{1}{2^3}, \frac{1}{2^4}, \dots, \frac{1}{2^{12}}$. Since the analytical value of $(-\Delta)^{\alpha/2} \phi(x)$ is not available, we examine the absolute value of the difference

$$\text{Diff}(h) = |(-\Delta)_h^{\alpha/2} \phi(x) - (-\Delta)_{\frac{h}{2}}^{\alpha/2} \phi(x)|,$$

and the log-log plot between $\text{Diff}(h)$ and the mesh size h to determine the order of accuracy. Fig. 1 confirms the second-order accuracy of $(-\Delta)_h^{\alpha/2}$ for $\alpha = 0.5, 1, 1.5$ respectively.

3 Structure of Physics-informed Neural Networks

In this section we elaborate the structure of the trapz-PiNNs. It consists of three main parts: training data, neural network solver, loss function and training algorithm.

Training data: We use the grid points $\mathcal{T} := \{(x_j, t_k) : 1 \leq j \leq J^n, 1 \leq k \leq K\}$, where $J = \frac{2}{h}$ and $K = \frac{T}{\Delta t}$, as training data, $(x_j)_j, (t_k)_k$ are uniform meshes for Ω and $(0, T)$ with mesh sizes h and Δt , respectively. Denote $(x_j)_j$ by Ω_h . Moreover, we can use validation data to monitor the training process and avoid overfitting phenomenon [24] and the validation data can be set as $\mathcal{V} := \Omega_h \times \{T_{\text{pred}}\}$.

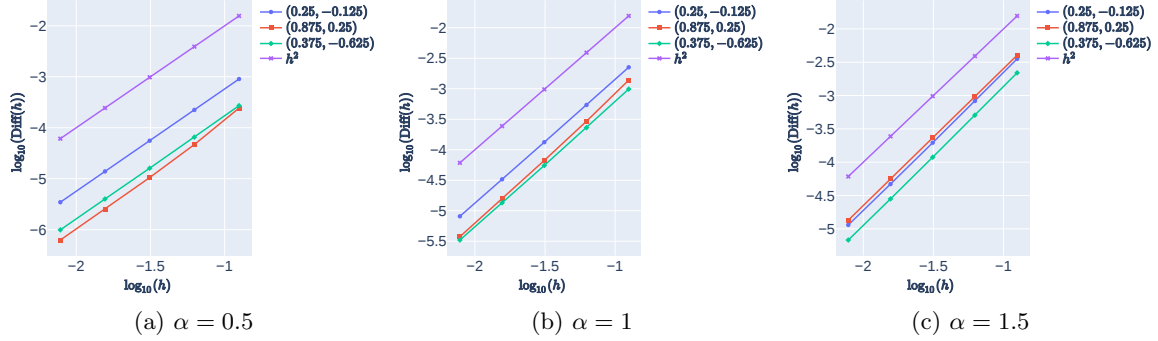


Figure 1: The accuracy of the approximation $(-\Delta)_h^{h/2}$ for the fractional laplacian by Eq. (12)

Neural Network solver: We use the fully-connected feedforward neural network (NN) in this paper, which is the foundation for all variants of neural networks [24]. It is also the core part of our NN solver Eq. (18). A NN u_{nn} with input dimension $d \in \mathbb{N}$, depth $N + 1 \in \mathbb{N}$ with N 's hidden layers, width $M \in \mathbb{N}$ and output dimension $d' \in \mathbb{N}$ is of the form

$$u_{nn}(x; \Theta) = A_{N+1} \circ \sigma \circ A_N \circ \sigma \circ A_{N-1} \circ \cdots \circ \sigma \circ A_1(x), \quad (16)$$

where

1. $A_1 : \mathbb{R}^d \rightarrow \mathbb{R}^M$, $A_i : \mathbb{R}^M \rightarrow \mathbb{R}^M$, $2 \leq i \leq N$ and $A_{N+1} : \mathbb{R}^M \rightarrow \mathbb{R}^{d'}$ are affine transformations with matrix representations

$$A_i(x) = W_i x + b_i, \quad i = 1, \dots, N + 1,$$

2. $\sigma : \mathbb{R} \rightarrow \mathbb{R}$ is a non-linear activation function. With some abuse of notation, we follow the convention that σ has the vectorized form $\sigma(x) = (\sigma(x_1), \dots, \sigma(x_n))$, $\forall x \in \mathbb{R}^n$, $\forall n \in \mathbb{N}$.
3. The (learnable) parameters Θ of NN in Eq. (16) are

$$\Theta := \{(W_i, b_i) : i = 1, \dots, N + 1\} \cong \mathbb{R}^{(N-1)M^2 + (N+d+d')M + d'}. \quad (17)$$

We call an NN has *shape* $(M, N + 1)$ if NN has width M and depth $N + 1$. To solve the FPE Eqs. (1) to (3), it is convenient to write the NN solver as an ansatz form

$$\hat{u}(x, t; \Theta) = \rho(t)\tau(x)u_{nn}(x, t; \Theta) + u_0(x), \quad (18)$$

so that \hat{u} satisfies the initial-boundary condition Eqs. (2) and (3). Here, $\rho(t)$ is a non-negative, bounded, strictly-increasing $C^\infty([0, \infty))$ function such that $\rho(0) = 0$ and $\tau(x)$ is a $C^\infty(\Omega)$ function with $\tau|_{\Omega^c} = 0$. The input and output dimensions of neural network $u_{nn}(t, x; \Theta)$ are $n + 1$ and 1 while the width and depth vary. A good choice of functions $\rho(t)$, $\tau(x)$ deserves careful consideration. We give a heuristic explanation here. The Universal Approximation Theorem [10, 12] guarantees that NN with arbitrary width bounded depth or bounded width arbitrary depth uniformly converges to continuous function on compact set in \mathbb{R}^n up to arbitrary degree of precision. By the ansatz form Eq. (18), the NN tries to learn

$$u_{nn}(t, x; \Theta) \xrightarrow{\Theta} \frac{u(t, x) - u_0(x)}{\rho(t)\tau(x)} =: \varphi(t, x), \quad (19)$$

where we assume $u \in C(\Omega_T)$ is the true solution and u_0 is the initial condition. Since Ω_T is open, we prefer φ can be continuously extended to the compact set $\overline{\Omega_T}$ so that $\varphi \in C(\overline{\Omega_T})$. This is possible if and only if ρ and τ are chosen such that φ has well-defined limiting behaviors as $x \rightarrow \partial\Omega$ and/or $t \rightarrow 0+$.

Loss function and training: The loss function $\mathbf{L}(\Theta)$ is the classic Mean Squared Error (MSE). We adopt the mini-batch training in this work, the loss function is therefore evaluated on a randomly selected training batch $\mathcal{B} \subset \mathcal{T}$ of fixed size in each epoch, i.e.

$$\mathbf{L}_{\mathcal{B}}(\Theta) = \frac{1}{|\mathcal{B}|} \sum_{(x_j, t_k) \in \mathcal{B}} |\partial_t \hat{u}(x_j, t_k; \Theta) - \mathcal{L}_h \hat{u}(x_j, t_k; \Theta)|^2. \quad (20)$$

\mathcal{L}_h denotes the discretized operator of \mathcal{L} at Eq. (1). In the RHS of Eq. (20), (partial) derivatives with integer order can be computed directly by automatic differentiation [7], fractional laplacian is evaluated by modified trapezoidal rule Eq. (12). The grid points for the trapezoidal rule coincide with training data \mathcal{T} . The NN solver at Eq. (18) already satisfied the initial and boundary conditions. Otherwise, proper loss functions with respect to initial and boundary conditions have to be added into Eq. (20). Once we set up the training data, NN solver and loss function, we are looking for best possible parameters Θ^* that minimize the loss function, i.e.

$$\Theta^* = \underset{\Theta}{\operatorname{arg\,min}} \mathbf{L}(\Theta). \quad (21)$$

To achieve this, we use ADAM, a popular stochastic gradient descent (SGD) algorithm [13]. Several hyperparameters are required to be initialized before running the algorithm. They are NN shape, batch size, learning rate, epoch, time and space resolutions. In addition, a initial guess Θ_0 is provided by Xavier Initialization scheme [6].

We summarize this section into the following Algorithm 1.

4 Numerical Experiments

In this section we demonstrate the expressive power of trapz-PiNNs. In each numerical examples, the trapz-PiNNs are trained on Ω_T with $T = 0.2$ for each equation and predict the solutions at multiple time steps starting from $t = 0.2$. Moreover, we verify the accuracy of DL solution by comparing with the reference solutions obtained from FDM together with modified trapezoidal rule Eq. (9) and determining the \mathcal{L}^2 relative error. We also investigate the DL solution profile from the pointwise absolute and relative errors.

Let \hat{u}, u_{ref} be the DL solution and reference solution, respectively. Recall that $\Omega_h = (x_j)_j$ is uniform mesh for Ω with mesh size h . Given a sample time t , the \mathcal{L}^2 relative error at t is defined by

$$\varepsilon = \sqrt{\frac{\sum_j |\hat{u}(x_j, t) - u_{\text{ref}}(x_j, t)|^2}{\sum_j |u_{\text{ref}}(x_j, t)|^2}} \quad (22)$$

Algorithm 1 Training algorithm for trapz-PiNN

Require: NN shape, batch size B , learning rate η , epoch K , space resolution h , time resolution Δt and initial parameter Θ_0 .

Ensure:

Initialize $\hat{u}(\cdot; \Theta_0)$, \mathcal{T} and \mathcal{V} .

for $i = 0, \dots, K - 1$ **do**

1. Randomly select $\mathcal{B} \in \mathcal{T}$ with $|\mathcal{B}| = B$
2. Compute

$$\nabla_{\Theta} \mathbf{L}_{\mathcal{B}}(\Theta)|_{\Theta=\Theta_i} = \nabla_{\Theta} \left\{ \frac{1}{|\mathcal{B}|} \sum_{(x_j, t_k) \in \mathcal{B}} |\partial_t \hat{u}(x_j, t_k; \Theta) - \mathcal{L}_h \hat{u}(x_j, t_k; \Theta)|^2 \right\} \Big|_{\Theta=\Theta_i}$$

3. Update $\Theta_{i+1} = \Theta_i - \eta \nabla_{\Theta} \mathbf{L}_{\mathcal{B}}(\Theta)|_{\Theta=\Theta_i}$ \triangleright This is vanilla SGD, we use ADAM in practice

4. Randomly select $\mathcal{B}' \in \mathcal{V}$ with $|\mathcal{B}'| = B$

5. Record the training error $\mathbf{L}_{\mathcal{B}}(\Theta_{i+1})$ and the validation error $\mathbf{L}_{\mathcal{B}'}(\Theta_{i+1})$. \triangleright For monitoring the training process

end for

and for each $x_j \in \Omega_h$, the absolute and relative errors at x_j are defined by

$$\epsilon_{\text{abs}}(x_j) = |\hat{u}(x_j, t) - u_{\text{ref}}(x_j, t)|, \quad (23)$$

$$\epsilon_{\text{re}}(x_j) = \left| \frac{\epsilon_{\text{abs}}(x_j, t)}{u_{\text{ref}}(x_j, t)} \right|. \quad (24)$$

The activation function σ , the functions $\rho(t)$ and $\tau(x)$ in the ansatz (18) are fixed throughout

$$\sigma(x) = \frac{1}{1 + \exp(-x)}, \quad \text{sigmoid function} \quad (25)$$

$$\rho(t) = 1 - \exp(-t), \quad (26)$$

$$\tau(x) = \left(\prod_{k=1}^n (1 - x_k^2)_+ \right)^{\frac{1}{2}}, \quad (27)$$

and the hyperparameters will be specified in each example. It worths mentioning that $\tau(x)$ is chosen a posterior to the initial condition.

To construct FDM reference solution for FPE Eqs. (1) to (3), we use grid points \mathcal{T} where, if not specified, space resolution $h = \frac{1}{32}$ and time step $\Delta t = \frac{h^2}{4}$. If any, first-order partial derivatives $\partial_{x_j} \{\cdot\}$, $j = 1, \dots, n$ are evaluated by classical upwind scheme, second-order partial derivatives $\partial_{x_i x_j}^2 \{\cdot\}$, $i, j = 1, \dots, n$ are discretized by central differences. Fractional laplacian is discretized by modified trapezoidal rule Eq. (9). For time evolution, we adopt third-order total-variation

diminishing Runge-Kutta scheme, i.e., given an ODE $\frac{du}{dt} = R(u)$,

$$\begin{aligned} U^{(1)} &= U^n + \Delta t R(U^n), \\ U^{(2)} &= \frac{3}{4}U^n + \frac{1}{4}U^{(1)} + \frac{1}{4}\Delta t R(U^{(1)}), \\ U^{(3)} &= \frac{1}{3}U^n + \frac{2}{3}U^{(2)} + \frac{2}{3}\Delta t R(U^{(2)}), \end{aligned}$$

where U^n denotes numerical solution of u evaluated at time $t = t_n$.

As a common practice, we adopt \mathcal{L}^2 relative error $\varepsilon = 0.01$ as benchmark. DL solution with \mathcal{L}^2 relative error $\varepsilon < 0.01$ is considered accurate in general. We call this accuracy by ε -accuracy. Another standard is attaining relative error $\epsilon_{\text{re}} < 1\%$ uniformly over domain. We stress that this is a very strict criteria for DL solvers in general and is hard to achieve in reality. One primary reason is that the DL solvers are optimized with respect to MSE, which itself is an indicator of global accuracy. To author's best knowledge, without utilizing external information such as incorporating high-fidelity simulated solution into loss function, there is no known loss function aiming for such high accuracy of (maximum) relative error.

All numerical experiments are coded in Python with machine learning package JAX [1] and performed on a Google Colab Pro+ account and the source codes are available at <https://github.com/sjiang23>.

4.1 Fractional Heat Equation

In both 2D and 3D, we consider the following fractional heat equation with the initial and boundary conditions:

$$\partial_t u(x, t) = -(-\Delta)^{\frac{\alpha}{2}} u(x, t), \quad (28)$$

$$u(x, 0) = c_n \left(\prod_{j=1}^n (1 - x_j^2)_+ \right)^4, \quad (29)$$

$$u(x, t) = 0, \quad x \notin (-1, 1)^n. \quad (30)$$

Here $n = 2, 3$, $c_2 = (\frac{315}{216})^2$ and $c_3 = (\frac{693}{512})^3$, where c_n are chosen so that $\int_{\mathbb{R}^n} u(x, 0) dx = 1$. It is not necessary to choose $u(x, 0)$ to be probability density and other choices are also feasible. We solve Eqs. (28) to (30) for $\alpha = 0.5, 1, 1.5$ in 2D and $\alpha = 1$ in 3D.

4.1.1 2D case

In 2D, the hyperparameters for trapz-PiNNs are chosen as the NN shape (20, 5), the learning rate 10^{-3} , the batch size 64, the epoch 2×10^5 , the space resolution $1/32$ and the time resolution 10^{-2} . Fig. 2a records the \mathcal{L}^2 relative errors ε defined in Eq. (22) at times steps $T + k/100, k = 0, \dots, 25$. Fig. 3 presents the FDM reference solutions, the DL solutions, the absolute error and relative error surfaces of the DL solutions, evaluated at time $t = 0.225$ for $\alpha = 0.5, 1, 1.5$. A detailed study of FDM numerical solution profile for Eqs. (28) to (30) in 2D can be found at [8].

From Fig. 2a, we observe that ε -accuracy is achieved starting from time $t = 0.2$ and is preserved into some time range of future for all values of α , in particular, the ε -accuracies stay less than 0.01 for longer period of time when the value of α is smaller. A possible contributing factor to this

behavior is that the solution of larger α departs further away from the initial conditions as shown in Figs. 3a, 3e and 3i. It is not surprising that the \mathcal{L}^2 relative errors for all values of α are strictly increasing with respect to time t , i.e., the closer to the training space Ω_T , the more accurate the DL solution and vice versa. The \mathcal{L}^2 relative error ε increases at fastest pace in time when $\alpha = 1.5$, comparing with those for $\alpha = 0.5, 1$. We also note that trapz-PiNN with the fixed NN shape (20, 5) is versatile enough to solve three different cases simultaneously while achieving reasonable accuracy.

Figs. 3a, 3e and 3i show the FDM solutions to fractional heat equations Eqs. (28) to (30) at time $t = 0.225$ for $\alpha = 0.5, 1, 1.5$ respectively, while Figs. 3b, 3f and 3j show the corresponding DL solutions. It is hard to recognize any difference between the FDM solutions and the DL solutions from the contour plots. Maximum absolute errors of the DL solutions are of the order 10^{-3} for all α . When $\alpha = 0.5$, Fig. 3c shows the absolute error at the corners of the domain Ω are much larger than that at other regions, Fig. 3d shows that a majority of Ω have relative errors strictly below 10^{-2} , in fact, 62.9% of the total area of Ω have relative errors $\epsilon_{re} < 1\%$. We also note that the relative errors close to corners are on the order of 10^{-1} and accounts for 5.7% of the area in total. In contrast, Figs. 3g and 3k show some points in the central area of Ω have the largest absolute errors for $\alpha = 1, 1.5$ respectively, while Figs. 3h and 3l show that these points have very low relative errors. Furthermore, 82.7% and 71.1% of Ω have relative errors $\epsilon_{re} < 1\%$. Similar to the case of $\alpha = 0.5$, relative errors above 10^{-1} appear at region close to corners and boundaries, making up 0.3% and 2.2% in total area for $\alpha = 1, 1.5$ respectively.

In general, high ε -accuracy indicates small relative errors for majority of the domain Ω . As can be seen from the reference solutions shown in Figs. 3a, 3e and 3i, the DL solutions at the regions with high relative errors have very small magnitude, compared with the interior region where the solutions have larger magnitude and small relative errors. It implies that, if true solution profile has different scales, trapz-PiNN predicts the region with moderate or large magnitude better than the region with small magnitude.

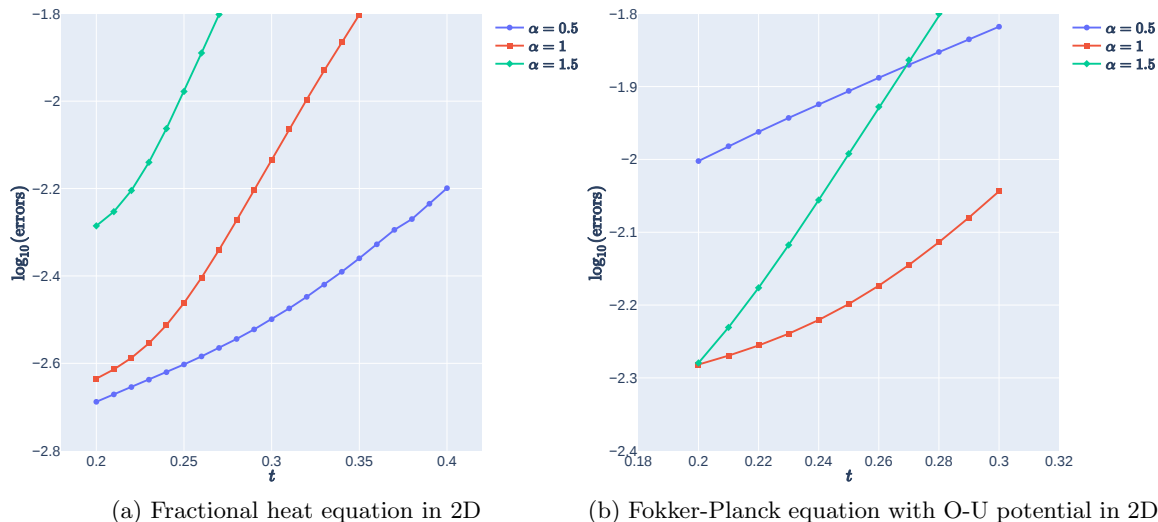


Figure 2: The \mathcal{L}^2 relative errors ε at time steps $0.2 + k/100, k = 0, \dots, 25$ for the DL solutions of (a) fractional heat equations in 2D (Eqs. (28) to (30)) and (b) FPEs with O-U potential in 2D (Eqs. (31) to (33)) when $\alpha = 0.5, 1, 1.5$.

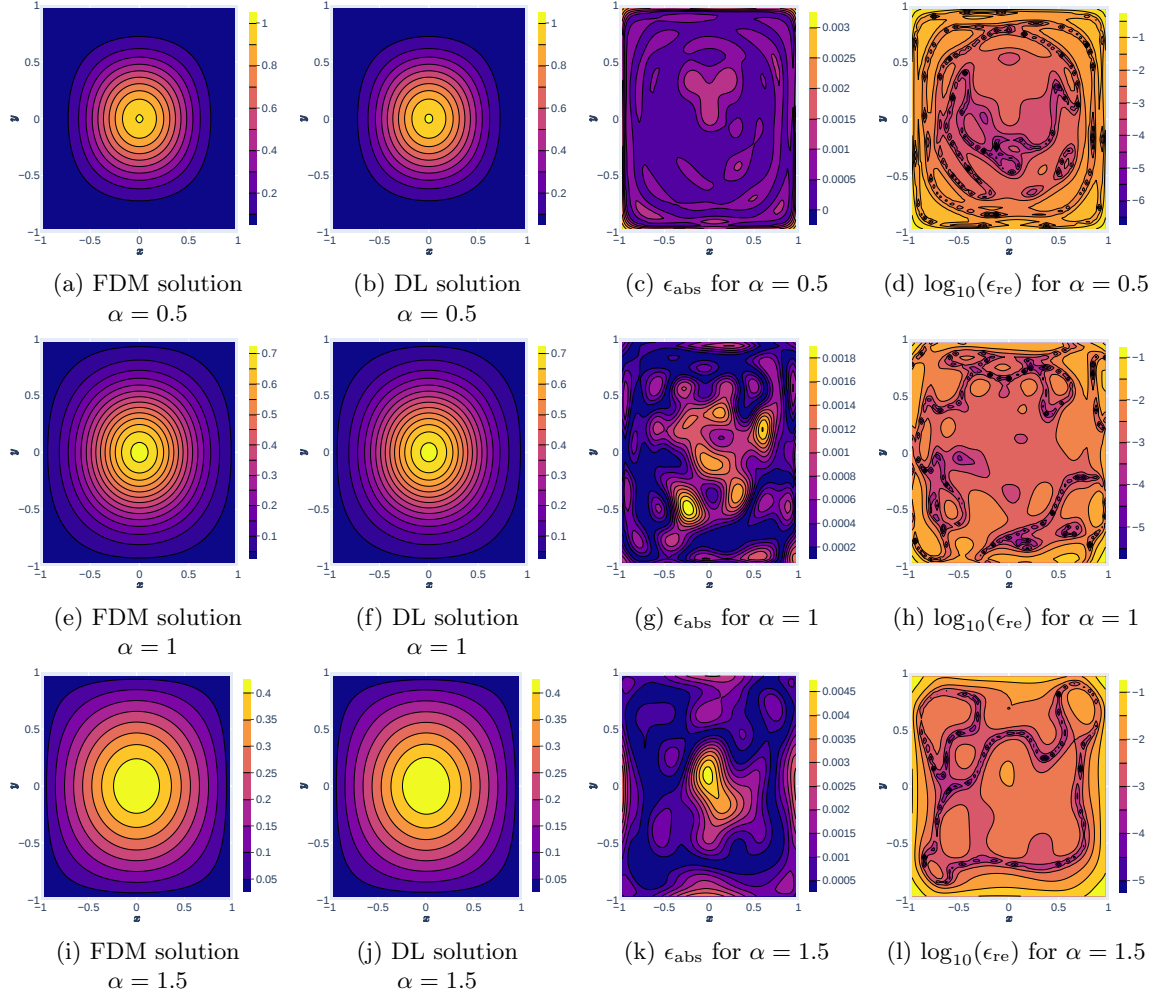


Figure 3: The contour plots of the FDM solutions, the DL solutions, the absolute and relative errors of the DL solutions for the fractional heat equations in 2D Eqs. (28) to (30) sampled at $t = 0.225$ for $\alpha = 0.5, 1, 1.5$.

4.1.2 3D case

In 3D, the hyperparameters for trapz-PiNN are chosen as the NN shape (20, 7), the learning rate 0.001, the epoch 3×10^5 , the batch size 100, the space resolution $1/20$ and the time resolution 0.01. The \mathcal{L}^2 relative errors ε at $t = 0.2 + k/100, k = 0, \dots, 5$ are recorded at Table 2. Fig. 4 presents the contour plots of the FDM and DL solutions, the absolute and relative errors of the DL solutions evaluated at $t = 0.21$ for the cross-sections $x_1 = -0.1$ and $x_2 = 0.85$, respectively. Due to the limitation of RAM, we use moderate space resolution $\frac{1}{20}$ for both FDM and DL solutions.

From Table 2, we observe that the ε -accuracy ($\varepsilon < 0.01$) is achieved starting from $t = 0.2$ and

preserved before $t = 0.25$. Similar to the 2D case, the FDM solutions shown in Figs. 4a and 4e and the corresponding DL solutions shown in Figs. 4b and 4f are indistinguishable. Fig. 4c shows the maximum absolute error ϵ_{abs} attained at some central points in the cross-section $x_1 = -0.1$. Fig. 4d shows that the majority of the cross-section have relative error below or around 10^{-2} . Fig. 4g also shows the absolute error peaks at some central points in the cross-section $x_2 = 0.85$. Fig. 4h shows the pointwise relative error ϵ_{re} at a significant part of the area close to the boundary of the cross-section $x_2 = 0.85$ is on the order of 10^{-1} while the other areas is below $10^{-1.5} \approx 3.2\%$. Furthermore, 76.1% of Ω have the relative error $\epsilon_{\text{re}} < 3\%$ while the regions with relative error $\epsilon_{\text{re}} > 10\%$ occupy 5.2% in Ω .

We see that moderate space resolution h reduces the size of training data \mathcal{T} and therefore the range of ε -accuracy, compared with the 2D counter-part. From Figs. 4d and 4h, we find that the cross-section $x_1 = -0.1$ has better overall accuracy than that of $x_2 = 0.85$, possibly since the latter one is closer to boundary of the cube Ω in \mathbb{R}^3 . We also know from the FDM solutions shown in Figs. 4a and 4e that the magnitude of solution profile for the cross-section $x_2 = 0.85$ is small. It follows again that trapz-PiNN predicts better in the region with moderate or large magnitude than region with small magnitude.

Table 2: The \mathcal{L}^2 relative errors ε at time steps $0.2 + k/100, k = 0, \dots, 5$ for the DL solutions of fractional heat equations in 3D (Eqs. (28) to (30)) with $\alpha = 1$

T_{pred}	$t = 0.2$	$t = 0.21$	$t = 0.22$	$t = 0.23$	$t = 0.24$	$t = 0.25$
\mathcal{L}^2 relative errors	6.856e-3	7.311e-3	7.838e-3	8.458e-3	9.196e-3	1.001e-2

4.2 FPEs with Ornstein–Uhlenbeck Potential in 2D

We consider the FPE with O-U potential in 2D:

$$\partial_t u(x, t) = -(\partial_1(x_1 u(x, t)) - \partial_2(x_2 u(x, t))) - (-\Delta)^{\frac{\alpha}{2}} u(x, t), \quad (31)$$

$$u(x, 0) = \left(\frac{315}{216}\right)^2 ((1 - x_1^2)(1 - x_2^2))_+^4, \quad (32)$$

$$u(x, t) = 0, \quad x \notin (-1, 1)^2, \quad (33)$$

with $\alpha = 0.5, 1, 1.5$. The solution u to the Fokker-Planck equation Eqs. (31) to (33) is the probability density function corresponding to the stochastic differential equations in 2D

$$dX_t = -X_t dt + dL_t^\alpha, \quad X_0 = X, \quad (34)$$

where L_t^α is the α -stable Lévy process and random variable X has distribution as $u(x, 0)$, with stochastic process vanishes outside domain Ω . Without the α -stable noise, the deterministic dynamical system drives the process to the unique stable point, the origin $(0, 0)$. Hyperparameters for trapz-PiNNs are chosen as the NN shape (20, 6), the learning rate 10^{-3} , the epoch 2×10^5 , the batch size 64, the space resolution $1/50$ and the time resolution 5×10^{-3} . Fig. 2b records the \mathcal{L}^2 relative errors ε at $t = 0.2 + k/100, k = 0, \dots, 10$. Fig. 5 presents the FDM and DL solutions and the absolute and relative error surfaces of the DL solutions evaluated at $t = 0.2$ for $\alpha = 0.5, 1, 1.5$ respectively. For more information on FDM numerical solution profile for equations Eqs. (31) to (33) in 2D, we refer to [8].

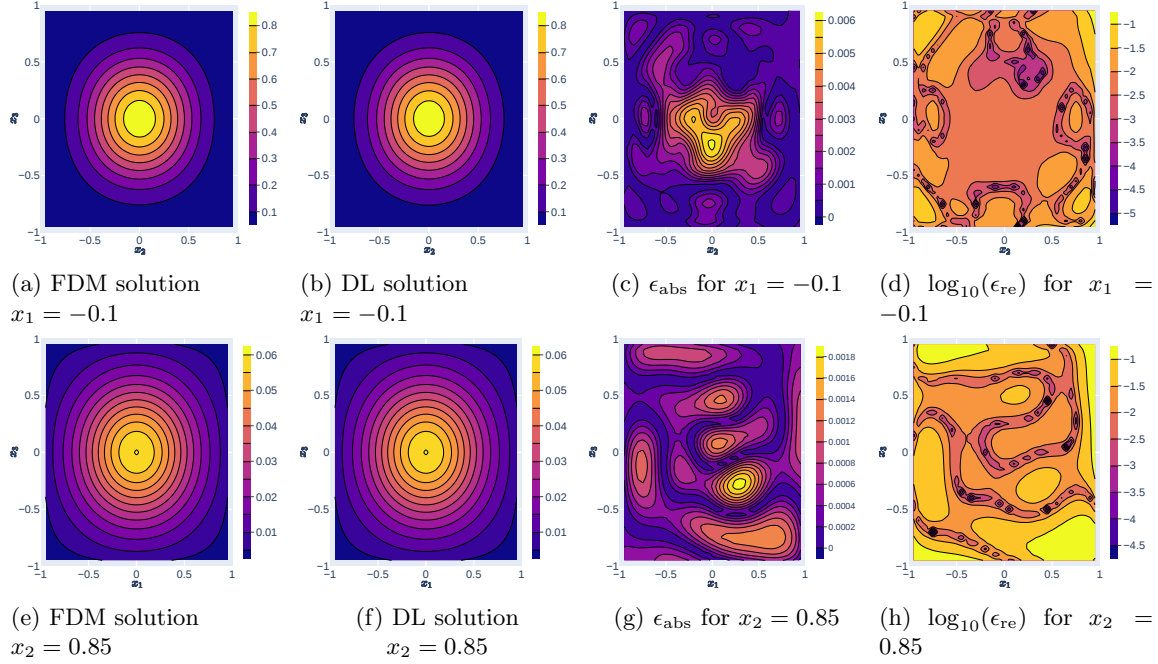


Figure 4: The contour plots of the FDM solutions, the DL solutions, the absolute and relative errors of the cross-sections $x_1 = -0.1$ and $x_2 = 0.85$ of the DL solutions for the fractional heat equations in 3D Eqs. (28) to (30) at $t = 0.21$ when $\alpha = 1$.

From Fig. 2b, we observe that the ε -accuracy ($\varepsilon < 0.01$) is achieved only at time $t = 0.2$ for $\alpha = 0.5$ under the effect of the O-U potential, on the other hand, the ε -accuracy is preserved up to time $t = 0.25$ for $\alpha = 1.5$ and up to $t = 0.3$ for $\alpha = 1$. \mathcal{L}^2 relative errors are increasing with respect to time t for all values of α . The rate of increase is highest for $\alpha = 1.5$.

Figs. 5a, 5e and 5i show the FDM solutions to Fokker-Planck equation with O-U potential in 2D Eqs. (31) to (33) at time $t = 0.2$ for $\alpha = 0.5, 1, 1.5$ respectively, while Figs. 5b, 5f and 5j are the corresponding DL solutions. They are hard to tell apart. When $\alpha = 0.5$, Fig. 5c shows maximum absolute error is of the order 10^{-2} and is attained at some interior points in the domain, Fig. 5d shows these peak points have the relative errors ϵ_{re} around $10^{-1.25} \approx 5.6\%$. Together with the FDM solution profile shown in Fig. 5a, we see that the area with the relative errors ϵ_{re} greater than 3% concentrates in the area with small magnitude (deep blue area) of the solution. When $\alpha = 0.5, 1$, Figs. 5g and 5k show the maximum absolute errors are below 5×10^{-3} . Together with the FDM solution profiles shown in Figs. 5e and 5i, Figs. 5h and 5l show the points attaining maximum absolute error have relative error below $10^{-1.5} \approx 3.2\%$. Furthermore, for $\alpha = 1$ and 1.5 , more than 76.9% and 80% of the total area has the relative error below 3% respectively and the area with large relative errors locates at the area with the solution of small magnitude. They account for 8.6% and 2.1% of the total area, respectively.

Under the effect of O-U potential, ε -accuracy and range of ε -accuracy are no longer similar to the case without O-U potential in Section 4.1.1. O-U potential drives the solution profile more higher at the origin and for $\alpha < 1$, it drives the profile near the boundary of the domain close to

zero [8]. This may explain the trapz-PiNN can predict accurately the solution for $\alpha = 0.5$ at $t = 0.2$ only but gives much better predictions for the cases of $\alpha = 1$ and 1.5.

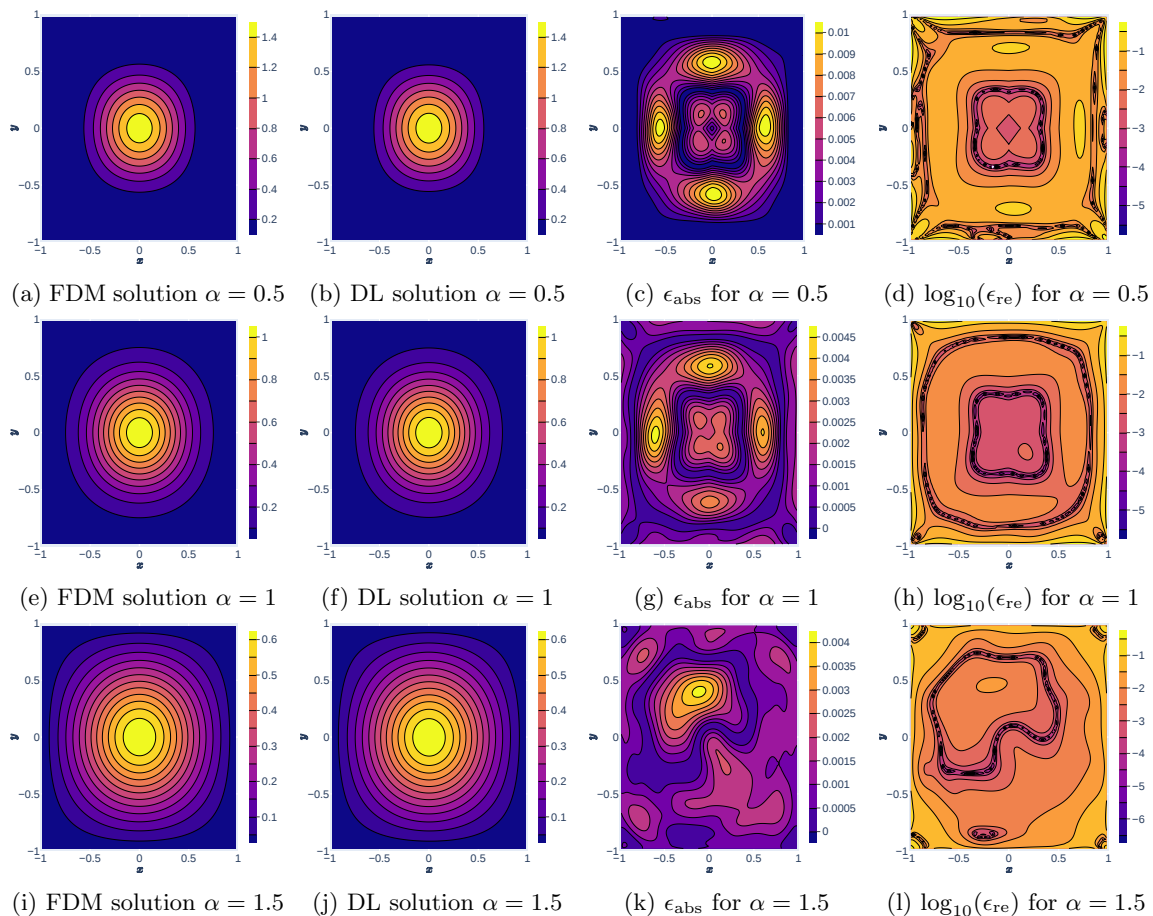


Figure 5: The contour plots of the FDM solutions, the DL solutions, the absolute and relative errors of DL solutions for FPE with O-U potential in 2D Eqs. (31) to (33) sampled at $t = 0.2$ for $\alpha = 0.5, 1, 1.5$.

4.3 A modified loss function

From the numerical results in Sections 4.1 and 4.2, we find that the trapz-PiNN is able to predict solutions with good overall accuracy and more accurate in the region with large or moderate magnitude than the region with small magnitude, when the true solution profile has different scales. The loss function MSE defined by Eq. (20) is a metric of global accuracy, rather than a pointwise one. If physical observations of solutions or high-fidelity simulated data is available, we propose an effective loss function to address above-mentioned issue.

Let $U(x, t)$ denote the physical observation or the high-fidelity simulated data at $(x, t) \in \Omega_T$

and \mathcal{B} be a training batch. The new loss function is defined by

$$\begin{aligned} \mathbf{L}_{\mathcal{B}}^{\text{new}}(\Theta) := & \frac{\lambda_1}{|\mathcal{B}|} \sum_{(x_j, t_k) \in \mathcal{B}} |\partial_t \hat{u}(x_j, t_k; \Theta) - \mathcal{L}_h \hat{u}(x_j, t_k; \Theta)|^2 \\ & + \frac{\lambda_2}{|\mathcal{B}|} \sum_{(x_j, t_k) \in \mathcal{B}} \left(\frac{|\hat{u}(x_j, t_k; \Theta) - U(x_j, t_k)| + \delta}{|U(x_j, t_k)| + \delta} \right)^2, \end{aligned} \quad (35)$$

where $\lambda_1, \lambda_2 > 0$ are constants, $\delta = 10^{-6}$ if U vanishes at some points in Ω_T , otherwise $\delta = 0$. One can see that the new loss function $\mathbf{L}_{\mathcal{B}}^{\text{new}}$ is a weighted sum of the loss function $\mathbf{L}_{\mathcal{B}}$ in Eq. (20) and the ‘mean-squared’ pointwise relative errors. To avoid repetitive presentation of the results in the same nature, we only study the Fokker-Planck equation with O-U potential when $\alpha = 0.5$ in this subsection. We compare the DL solutions computed by trapz-PiNN with two loss functions through pointwise absolute and relative errors. To have a fair comparison, we remain using the same set of hyperparameters chosen in Section 4.2. We refer trapz-PiNNs equipped with the loss functions $\mathbf{L}_{\mathcal{B}}$ at Eq. (20) and $\mathbf{L}_{\mathcal{B}}^{\text{new}}$ at Eq. (35) as the original and the new trapz-PiNN, respectively. The high-fidelity simulated data are the FDM solutions evaluated at $t = 0.01 + k/100$, $k = 0, \dots, 19$. Fig. 6 shows the comparison between the DL solutions predicted at $t = 0.2$ by the original and new trapz-PiNNs.

From Figs. 6a and 6b, we can see that the new trapz-PiNN reduces the maximum absolute error ϵ_{abs} from 0.01 to 0.006. Moreover, as shown in Figs. 6c and 6d, the pointwise relative errors ϵ_{re} for the new trapz-PiNN decreases to 3% at majority of the total area from the order of 10% corresponding to the original trapz-PiNN. More precisely, 61.3% of the total area has the pointwise relative error ϵ_{re} below 3%. In comparison, only 40.7% of the area achieves such accuracy for the original trapz-PiNN. The \mathcal{L}^2 relative error ε for the DL solution predicted by the new trapz-PiNN is 5.8×10^{-3} while the original trapz-PiNN attains $\varepsilon = 9.9 \times 10^{-3}$. The range of ε -accuracy of the new trapz-PiNN extended from $t = 0.2$ to at least beyond $t = 0.21$, as the \mathcal{L}^2 relative error at $t = 0.21$ is $\varepsilon = 6.1 \times 10^{-3}$.

The new loss function improves the performance of the trapz-PiNN on pointwise absolute and relative errors and extends the range of ε -accuracy. Smaller maximum relative error can be achieved if larger NN shape and longer epoch are chosen. If physical observations or high-fidelity simulation is available, using the new loss function can achieve higher global and local accuracies.

5 Conclusion

We propose trapz-PiNN, a new physics-informed neural network, based on a recently developed modified trapezoidal rule, to solve non-local Fokker-Planck equations involving fractional laplacian. We have presented the simplest version of the modified trapezoidal rule in \mathbb{R}^n and have verified second order accuracy for computing fractional laplacian in 2D. We have demonstrated trapz-PiNNs have high expressive power through numerical examples on fractional heat equations in 2D and 3D and Fokker-Planck equation with O-U potential in 2D. The DL solutions that has low \mathcal{L}^2 relative error (ε -accuracy) in general guarantee a small pointwise relative error for areas with high or moderate magnitude in Ω . We also observe that trapz-PiNNs have some range of ε -accuracy for almost all cases we studied. If physical observation or high-fidelity simulation of true solution is available, we propose an effective loss function integrating the extra information so that trapz-PiNN improves the performance on local metrics such as pointwise absolute and relative errors.

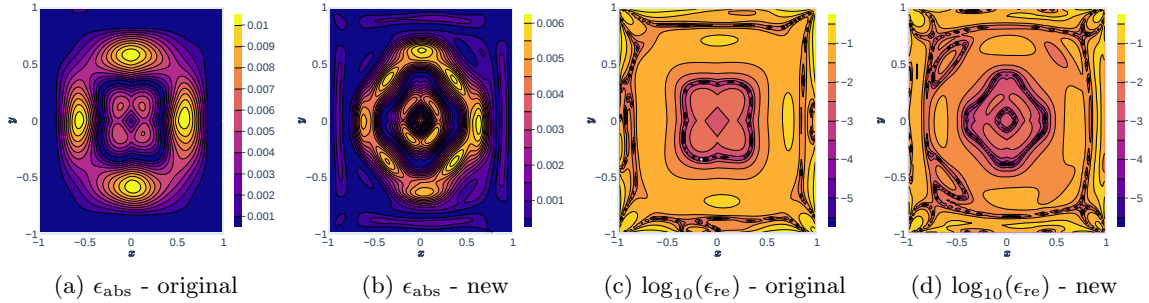


Figure 6: The contour plots of the absolute and relative errors of the DL solutions computed by the original and the new trapz-PiNN, for FPE with O-U potential in 2D Eqs. (31) to (33) sampled at $t = 0.2$ for $\alpha = 0.5$.

There are numerous questions remain to be investigated in future. Without resorting to using more brute force training or adopting external information, we will focus on designing an effective loss function to control the relative errors from region with vanishing magnitude, especially for PDEs with multi-scale solution profile. Due to RAM restriction, we only use moderate space resolution in solving fractional heat equation in 3D at Section 4.1.2. Low-memory fast algorithm for numerical fractional laplacian by modified trapezoidal rule has been developed and implemented in [21, 8]. One can incorporate this fast algorithm into deep learning algorithm to alleviate the “curse of dimensionality”. We are also interested in developing efficient trapz-PiNNs for Fokker-Planck equation Eq. (1) with discontinuous initial condition at boundary or with natural boundary (unbounded) condition.

6 Acknowledgement

The authors thanks Yiwei Wang for very helpful discussion about this work.

References

- [1] James Bradbury, Roy Frostig, Peter Hawkins, Matthew James Johnson, Chris Leary, Dougal Maclaurin, George Necula, Adam Paszke, Jake VanderPlas, Skye Wanderman-Milne, and Qiao Zhang. JAX: composable transformations of Python+NumPy programs, 2018.
- [2] P. D. Ditlevsen. Observation of alpha-stable noise induced millennial climate changes from an ice-core record. In *AGU Fall Meeting Abstracts*, volume 2005, pages NG23B-0097, December 2005.
- [3] J. Duan. *An Introduction to Stochastic Dynamics*. Cambridge Texts in Applied Mathematics. Cambridge University Press, 2015.
- [4] Siwei Duo and Yanzhi Zhang. Accurate numerical methods for two and three dimensional integral fractional laplacian with applications. *Computer Methods in Applied Mechanics and Engineering*, 355:639–662, 2019.

- [5] Ting Gao, Jinqiao Duan, and Xiaofan Li. Fokker–Planck equations for stochastic dynamical systems with symmetric Lévy motions. *Applied Mathematics and Computation*, 278(Supplement C):1 – 20, 2016.
- [6] Xavier Glorot and Yoshua Bengio. Understanding the difficulty of training deep feedforward neural networks. In *Proceedings of the thirteenth international conference on artificial intelligence and statistics*, pages 249–256. JMLR Workshop and Conference Proceedings, 2010.
- [7] A. Griewank and A. Walther. *Evaluating Derivatives: Principles and Techniques of Algorithmic Differentiation, Second Edition*. Other Titles in Applied Mathematics. Society for Industrial and Applied Mathematics (SIAM, 3600 Market Street, Floor 6, Philadelphia, PA 19104), 2008.
- [8] Hansen Ha. *Non-Gaussian Stochastic Dynamics with Deterministic Numerical Tools*. PhD thesis, 2018. Copyright - Database copyright ProQuest LLC; ProQuest does not claim copyright in the individual underlying works; Last updated - 2018-11-22.
- [9] Jiequn Han, Arnulf Jentzen, and Weinan E. Solving high-dimensional partial differential equations using deep learning. *Proceedings of the National Academy of Sciences*, 115(34):8505–8510, 2018.
- [10] Kurt Hornik. Approximation capabilities of multilayer feedforward networks. *Neural Networks*, 4(2):251–257, 1991.
- [11] Senbao Jiang and Xiaofan Li. Arbitrarily high-order trapezoidal rules for functions with fractional singularities in two dimensions. *Applied Mathematics and Computation*, 429:127236, 2022.
- [12] Patrick Kidger and Terry Lyons. Universal approximation with deep narrow networks. In *Conference on learning theory*, pages 2306–2327. PMLR, 2020.
- [13] Diederik P Kingma and Jimmy Ba. Adam: A method for stochastic optimization. *arXiv preprint arXiv:1412.6980*, 2014.
- [14] Anna Lischke, Guofei Pang, Mamikon Gulian, Fangying Song, Christian Glusa, Xiaoning Zheng, Zhiping Mao, Wei Cai, Mark M. Meerschaert, Mark Ainsworth, and George Em Karniadakis. What is the fractional laplacian? a comparative review with new results. *Journal of Computational Physics*, 404:109009, 2020.
- [15] G. Pang, M. D’Elia, M. Parks, and G.E. Karniadakis. nPINNs: Nonlocal physics-informed neural networks for a parametrized nonlocal universal laplacian operator. algorithms and applications. *Journal of Computational Physics*, 422:109760, 2020.
- [16] Guofei Pang, Lu Lu, and George Karniadakis. fPINNs: Fractional physics-informed neural networks. *SIAM Journal on Scientific Computing*, 41(4):A2603–A2626, 2019.
- [17] M. Raissi, P. Perdikaris, and G.E. Karniadakis. Physics-informed neural networks: A deep learning framework for solving forward and inverse problems involving nonlinear partial differential equations. *Journal of Computational Physics*, 378:686–707, 2019.
- [18] James A Roberts, Tjeerd W Boonstra, and Michael Breakspear. The heavy tail of the human brain. *Current opinion in neurobiology*, 31:164–172, 2015.

- [19] Xiaorong Shen, Hao Zhang, Yong Xu, and Suxia Meng. Observation of alpha-stable noise in the laser gyroscope data. *IEEE Sensors Journal*, 16(7):1998–2003, 2016.
- [20] Justin Sirignano and Konstantinos Spiliopoulos. Dgm: A deep learning algorithm for solving partial differential equations. *Journal of Computational Physics*, 375:1339–1364, 2018.
- [21] Hong Wang and Treena S. Basu. A fast finite difference method for two-dimensional space-fractional diffusion equations. *SIAM Journal on Scientific Computing*, 34(5):A2444–A2458, 2012.
- [22] Hong Wang and Ning Du. A fast finite difference method for three-dimensional time-dependent space-fractional diffusion equations and its efficient implementation. *Journal of Computational Physics*, 253:50–63, 2013.
- [23] Yong Xu, Hao Zhang, Yongge Li, Kuang Zhou, Qi Liu, and Jürgen Kurths. Solving Fokker-Planck equation using deep learning. *Chaos: An Interdisciplinary Journal of Nonlinear Science*, 30(1):013133, 2020.
- [24] Aston Zhang, Zachary C. Lipton, Mu Li, and Alexander J. Smola. Dive into deep learning. *arXiv preprint arXiv:2106.11342*, 2021.
- [25] Dongkun Zhang, Ling Guo, and George Em Karniadakis. Learning in modal space: Solving time-dependent stochastic pdes using physics-informed neural networks. *SIAM Journal on Scientific Computing*, 42(2):A639–A665, 2020.
- [26] Meng Zhao, Hong Wang, and Aijie Cheng. A fast finite difference method for three-dimensional time-dependent space-fractional diffusion equations with fractional derivative boundary conditions. *Journal of Scientific Computing*, 74(2):1009–1033, 2018.